Publication VI

Tero Hottinen, Olli Himanen, Suvi Karvonen, Iwao Nitta, ”*Inhomogeneous compression of PEMFC gas diffusion layer Part II. Modeling the effect*”, Journal of Power Sources 171, pp. 113-121, 2007

Available online at www.sciencedirect.com
ScienceDirect
Journal of Power Sources 171 (2007) 113–121
JOURNAL OF POWER SOURCES
www.elsevier.com/locate/jpowsour

Inhomogeneous compression of PEMFC gas diffusion layer Part II. Modeling the effect

Tero Hottinen *, Olli Himanen, Suvi Karvonen, Iwao Nitta

Helsinki University of Technology, Laboratory of Advanced Energy Systems, P.O. Box 2200, Fin-02015 Hut, Finland

Received 4 September 2006; received in revised form 19 October 2006; accepted 31 October 2006
Available online 30 November 2006

Abstract

The effect of inhomogeneous compression of GDL on the mass and charge transfer in PEMFC is studied. The model utilizes experimentally evaluated GDL parameters as a function of thickness. The modeling results are compared with a conventional model that excludes the effects. As a result, it is shown that the inhomogeneous compression has a significant effect on the current density distribution because of the varying contact resistance between GDL and electrode. This also implies that there are possible hot spots occurring inside the electrode, and thus inhomogeneous compression can have significant effects on the lifetime and local performance of the cell. According to the achieved results, the inhomogeneous compression of GDL cannot be neglected.

Keywords: PEMFC; Modeling; Gas diffusion layer; Inhomogeneous compression; Contact resistance; Current density distribution

1. Introduction

Fuel cells are electrochemical devices that convert the chemical energy of reactants directly into electricity and heat. Due to their advantageous properties, such as potential for high energy density and low environmental emissions, fuel cells are believed to gain significant market in the near future. The main applications for fuel cells are automotive, stationary, and portable power production. The large-scale market penetration of fuel cells still requires cost and performance improvements. In order to achieve these improvements, it is essential to have a deep insight into the processes occurring inside the cell and its components.

One of the key components affecting the performance of a polymer electrolyte membrane fuel cell (PEMFC) is the gas diffusion layer (GDL). GDLs have to provide several functions for the fuel cell operation: a passage for reactant access and excess product water removal to and from the electrodes, electronic conductivity, heat removal, and adequate mechanical support for the membrane electrode assembly (MEA). GDLs are typically made of highly porous carbon-fiber based paper or cloth in order to fulfill these requirements. High porosity gives a characteristic soft and brittle structure for the GDLs, which causes a deformation in its shape when the fuel cell is assembled and components compressed together.

The physical properties of GDL are changed under compression, and thus also its mass, heat, and charge transfer properties are changed. Any change in physical properties of GDL in order to improve the charge transport may cause an adverse effect on the mass transport and vice versa. It has been experimentally shown that changes in the properties can have a significant effect on the fuel cell performance, see e.g. [1,2]. It is particularly worth noting that the deformation of GDL is not homogeneous. The parts of the GDL situated under the current collecting rib of the flow-field plate are significantly more compressed than the parts under the channel. This inhomogeneous compression may cause significant changes in the local physical properties of GDL, and thus also in the local cell performance by changing the local reactant and current profiles.

Even though it has been known for some time that the inhomogeneous compression of GDL may have a significant effect

* Corresponding author. Current address: Wärtsilä Corporation, Fuel Cells, Tekniikantie 14, 02150 Espoo, Finland. Tel.: +358 44 5838253; fax: +359 10 7099616.
E-mail address: tero.hottinen@wartsila.com (T. Hottinen).

0378-7753/$ – see front matter © 2006 Elsevier B.V. All rights reserved.
doi:10.1016/j.jpowsour.2006.10.076

Nomenclature

c	concentration (mol m^{-3})
d	channel and rib width (m)
D	diffusion coefficient (m^2 s^{-1})
$\vec{e}$	unit vector
E_0	reversible cell potential (V)
F	Faraday constant (A s mol^{-1})
h	thickness (m)
i	current density (A m^{-2})
j	current production rate (A m^{-3})
j_0	exchange current density (A m^{-3})
k	permeability (m^2)
M	molar mass (kg mol^{-1})
$\vec{N}$	molar flux (mol m^{-2} s^{-1})
p	pressure (Pa)
r	resistance (Ω m^2)
R	gas constant (J mol^{-1} K^{-1})
s	liquid water saturation
T	temperature (K)
$\vec{v}$	velocity (m s^{-1})
X	molar fraction
z	number of transferred electrons

Greek letters

α_r	reaction symmetry factor
ε	porosity
η	overpotential (V)
μ	viscosity (kg m^{-1} s^{-1})
ρ	density (kg m^{-3})
σ	conductivity (Ω^{-1} m^{-1})
ϕ	electronic potential (V)
ϕ_m	protonic potential (V)

Subscripts

a	anode
ave	average
c	cathode
comp	compressed
cont,e	contact between GDL and electrode
cont,gr	contact between GDL and graphite
e	electrode
eff	effective
GDL	gas diffusion layer
H_2O	water
min	minimum
N_2	nitrogen
O_2	oxygen
ref	reference
sat	saturation
x	x-direction, in-plane
y	y-direction, through-plane

on the cell performance, most of the PEMFC modeling studies have neglected this effect. Zhou et al. [3] investigated the effect that the shape of the current collecting rib has on the changes in porosity of GDL and contact resistance between rib and GDL. Sun et al. [4] studied the effect that the inhomogeneous compression of GDL, affecting the local porosity and conductivity, has on the fuel cell performance and local current density distribution. Even though they assumed a fairly small value for the compression (15%) and neglected the permeability and contact resistance effects, they concluded that the inhomogeneous compression affected the local current density distribution notably. Sui and Djilali [5] varied only the values of through-plane conductivity and diffusivity of GDL, and observed that the changes in local values affect the current density profile.

This second part of this contribution focuses on modeling the effect that inhomogeneous compression of GDL has on local species and current distributions. The model utilizes experimentally evaluated parameter values as a function of GDL thickness. These values are taken from the first part of this study, which focused on the ex-situ experimental evaluation of the GDL parameters [6]. The modeling results are compared with a conventional model that excludes the effects of inhomogeneous compression, and assumes the GDL parameters constant. The comparison gives insight into how the inhomogeneous compression of GDL affects the local cell performance.

2. Model

Two different cases are modeled: one with homogeneous properties of GDL (referred to as 'base case') and one where the inhomogeneous compression of GDL is taken into account. The used geometry is a 2D cross-section of the cell, and the modeled geometries are illustrated in Fig. 1. The model consists of the anode and cathode GDLs and electrodes, and the membrane. The ribs and channels of the flow-field plates are accounted for as boundary conditions. Only half-widths of the rib and channel structure and components below them are modeled, and the left and right geometry edges of Fig. 1 (boundaries III–VII) are modeled with symmetry boundary conditions, i.e. it is assumed that the cell geometry continues symmetrically to both directions.

The model takes into account the charge and multicomponent mass transfer in the cathode GDL and electrode, and charge transfer in the membrane and anode GDL and electrode. The main assumptions of the model are that water may exist in two phases but the transfer of liquid phase is similar to gas phase, i.e. equations for capillary movement are not included. In addition, the anode activation and mass transfer limitations are assumed to be negligible, and the cell is treated as isothermal. Even though the effects of inhomogeneous compression are taken into account also at the anode, the intrusion of the GDL into the channel is not included in the modeled geometry. This is made for simplicity, because the inclusion of it has an insignificantly small effect on the current profile of the anode GDL only. The details of the model are described in the following subchapters.

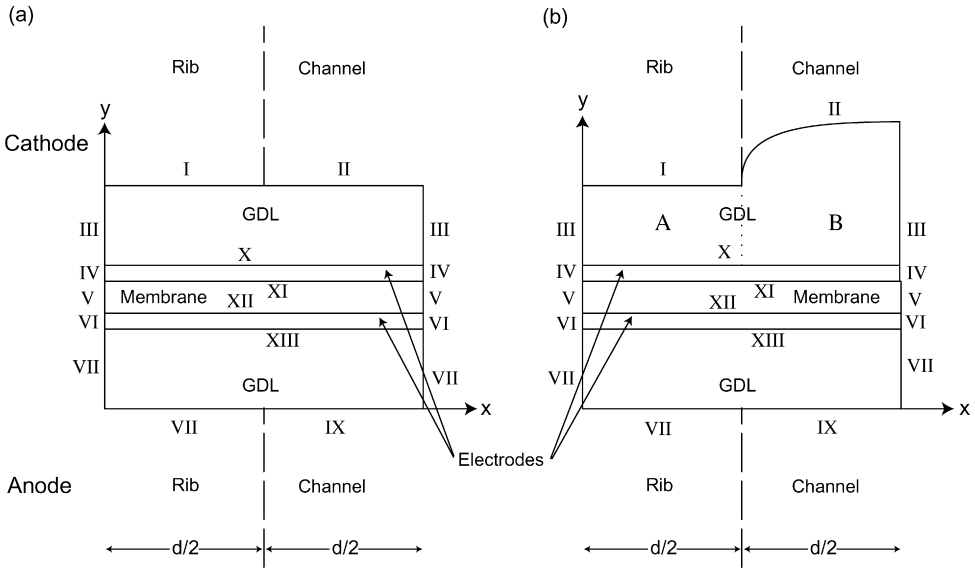

Fig. 1. Modeling domains: (a) geometry with homogeneous compression of GDL (base case); (b) geometry with inhomogeneous compression of GDL taken into account. Roman numerals refer to the boundaries of the modeled geometries. The domains representing different cell components are not in scale in the figure.

2.1. Equations

2.1.1. Cathode GDL

The governing equations at the cathode GDL are the conservation of mass, momentum, species, and charge listed in Eqs. (1)–(4), respectively:

$$\nabla \cdot (\rho \vec{v}) = 0 \tag{1}$$

$$\nabla p = -\frac{\mu}{k}\vec{v} \tag{2}$$

$$\nabla \cdot \vec{N}_i = 0 \tag{3}$$

$$\nabla \cdot \left(-\sigma_{\mathrm{GDL},x} \frac{\partial \phi_{\mathrm{GDL,c}}}{\partial x}\vec{e}_x - \sigma_{\mathrm{GDL},y} \frac{\partial \phi_{\mathrm{GDL,c}}}{\partial y}\vec{e}_y \right) = 0 \tag{4}$$

where different in-plane and through-plane conductivities of GDL are presented with subscripts x and y, respectively.

The multicomponent mass transfer of different species (oxygen, water, and nitrogen) takes into account the convective and diffusive mass fluxes. The species flux equation is

$$\begin{bmatrix} \vec{N}_{\mathrm{O_2}} \\ \vec{N}_{\mathrm{H_2O}} \end{bmatrix} = c\vec{v} \begin{bmatrix} X_{\mathrm{O_2}} \\ X_{\mathrm{H_2O}} \end{bmatrix} - c\bar{D}_{\mathrm{eff}} \begin{bmatrix} \nabla X_{\mathrm{O_2}} \\ \nabla X_{\mathrm{H_2O}} \end{bmatrix} \tag{5}$$

Concentration and density of the gas mixture are calculated from the ideal gas law:

$$c = \frac{p}{RT} \tag{6}$$

and

$$\rho = \frac{pM}{RT} \tag{7}$$

where M is the molar mass of the gas mixture defined as

$$M = \sum_i X_i M_i \tag{8}$$

$\bar{D}_{\mathrm{eff}}$ in Eq. (5) is the effective multicomponent diffusion coefficient tensor corrected by the Bruggeman correlation to take the effect of porosity and tortuosity into account:

$$\bar{D}_{\mathrm{eff}} = (\varepsilon(1-s))^{1.5}\bar{D} \tag{9}$$

The effect of porosity reduction due to liquid water saturation, s, is also accounted for. The saturation s is defined as the fraction of pores occupied by liquid water, i.e. the molar fraction of water exceeding the corresponding saturation molar fraction:

$$X_{\mathrm{sat}} = \frac{p_{\mathrm{sat}}}{p} \tag{10}$$

The saturation pressure of water can be calculated as [7]:

$$\log_{10}(p_{\mathrm{sat}}\,(\mathrm{bar})) = 28.59051 - 8.2\,\log(T + 0.01) + 0.0024804(T + 0.01) - \frac{3142.31}{T + 0.01} \tag{11}$$

which gives the saturation pressure in bar. The components of multicomponent diffusion coefficient tensor $\bar{D}$ are calculated from binary Maxwell–Stefan diffusion coefficients as [8]:

$$\begin{aligned} D_{11} &= D_{\mathrm{O_2,N_2}} \frac{X_{\mathrm{O_2}} D_{\mathrm{H_2O,N_2}} + (1 - X_{\mathrm{O_2}}) D_{\mathrm{O_2,H_2O}}}{S}, \\ D_{12} &= X_{\mathrm{O_2}} D_{\mathrm{H_2O,N_2}} \frac{D_{\mathrm{O_2,N_2}} - D_{\mathrm{O_2,H_2O}}}{S}, \\ D_{11} &= X_{\mathrm{H_2O}} D_{\mathrm{O_2,N_2}} \frac{D_{\mathrm{H_2O,N_2}} - D_{\mathrm{O_2,H_2O}}}{S}, \\ D_{22} &= D_{\mathrm{H_2O,N_2}} \frac{X_{\mathrm{H_2O}} D_{\mathrm{O_2,N_2}} + (1 - X_{\mathrm{H_2O}}) D_{\mathrm{O_2,H_2O}}}{S}, \\ S &= X_{\mathrm{O_2}} D_{\mathrm{H_2O,N_2}} + X_{\mathrm{H_2O}} D_{\mathrm{O_2,N_2}} + X_{\mathrm{N_2}} D_{\mathrm{O_2,H_2O}} \end{aligned} \tag{12}$$

In addition, the pressure and temperature corrections for binary diffusion coefficients are used [9]:

$$D_{i,j} = \frac{p_0}{p}\left(\frac{T}{T_0}\right)^{1.5} D^0_{i,j} \tag{13}$$

The molar fraction of nitrogen is calculated knowing that the molar fractions sum up to unity:

$$X_{N_2} = 1 - X_{H_2O} - X_{O_2} \tag{14}$$

2.1.2. Cathode electrode

The governing equations for the cathode electrode are the same as for cathode GDL with the exception that the conservation equations of mass, species and charge have source terms. The mass and species equations have source terms because of the oxygen consumed and water produced in the fuel cell reactions, and charge equation because the protonic current is changed into electronic current. Thus, these conservation equations are rewritten as in Eqs. (15)–(19):

$$\nabla \cdot (\rho \vec{v}) = -\frac{j_c M_{O_2}}{4F} + \frac{j_c M_{H_2O}}{2F} \tag{15}$$

$$\nabla \cdot \vec{N}_{O_2} = -\frac{j_c}{4F} \tag{16}$$

$$\nabla \cdot \vec{N}_{H_2O} = \frac{j_c}{2F} \tag{17}$$

$$\nabla \cdot (-\sigma_e \nabla \phi_{e,c}) = j_c \tag{18}$$

$$\nabla \cdot (-\sigma_m \nabla \phi_m) = -j_c \tag{19}$$

The current production due to electrochemical reactions at the cathode is calculated from the Butler–Volmer equation:

$$j_c = j_{0,c} \frac{c_{O_2}}{c^{ref}_{O_2}} \exp\left(\frac{-\alpha_r F}{RT}\eta\right) \tag{20}$$

The reference oxygen concentration is taken to be the case where only pure oxygen is present at the electrode, and thus the concentration term in the Butler–Volmer equation can be approximated as the molar fraction of oxygen, i.e.:

$$\frac{c_{O_2}}{c^{ref}_{O_2}} = X_{O_2} \tag{21}$$

The cathode overpotential in Eq. (19) is defined as

$$\eta = \phi_{e,c} - \phi_m - E_0 \tag{22}$$

2.1.3. Cathode boundary conditions

The electronic potential of the cathode decreases at the interface between gas diffusion layer and electrode due to contact resistance. The potentials of electrode and gas diffusion layer are related to each other through the current density passing the interface by Ohm's law giving a condition for both electrode and gas diffusion layer potentials at boundary X:

$$i = -\sigma_{GDL,y}\frac{\partial \phi_{GDL,c}}{\partial y} = -\sigma_e \frac{\partial \phi_{e,c}}{\partial y} = \frac{\phi_{e,c} - \phi_{GDL,c}}{r_{cont,e}} \tag{23}$$

The potential loss in the current collector is assumed to be negligible, and thus the only loss between the gas diffusion layer and current collector is due to contact resistance. Similarly as in Eq. (23) the contact resistance between the current collecting rib and GDL at boundary I yields:

$$i = -\sigma_{GDL,y}\frac{\partial \phi_{GDL,c}}{\partial y} = \frac{\phi_{GDL,c} - \phi_{0,c}}{r_{cont,gr}} \tag{24}$$

No electronic current passes through the interfaces between the GDL and the channel (boundary II), and electrode and membrane (boundary XI), and thus

$$\frac{\partial \phi_{GDL,c}}{\partial y} = \frac{\partial \phi_{e,c}}{\partial y} = 0 \tag{25}$$

The protonic potential is set continuous over boundary XI because it is assumed that there is no contact resistance for protonic current between membrane and electrode. Gas diffusion layer does not conduct protons, and thus no protonic current passes through boundary X yielding:

$$\frac{\partial \phi_m}{\partial y} = 0 \tag{26}$$

It is assumed that the gas mixture is at ambient pressure in the channel and that the gas mixture is always ideally mixed, leading into fixed boundary conditions for pressure and species molar fractions at boundary II. Typically in 2D models, a standard value of 0.21 is used for molar fraction of oxygen. However, such a condition exists only at the very beginning of the inlet channel where no oxygen has been consumed, or when an infinite air stoichiometry is used. For this reason, it is assumed here that the molar fraction of oxygen corresponds to the average value in the middle of the channel when dry air with a stoichiometry of 2 is fed into the cell. This leads into fixed values of approximately 0.153 and 0.077 for oxygen and water molar fractions, respectively. The fixed molar fraction of nitrogen at boundary II is calculated from Eq. (14).

There is no mass transfer at the interfaces between the gas diffusion layer and current collecting rib (boundary I), and electrode and membrane (boundary XI), and thus

$$\vec{v} \cdot \vec{e}_y = 0 \tag{27}$$

$$\vec{N}_i \cdot \vec{e}_y = 0 \tag{28}$$

Because the anode side mass transfer was neglected, it is assumed for simplicity that also the water does not penetrate the membrane.

Finally, symmetry boundary conditions are applied on the boundaries III and IV, i.e.:

$$\vec{v} \cdot \vec{e}_x = 0 \tag{29}$$

$$\vec{N}_i \cdot \vec{e}_x = 0 \tag{30}$$

$$\frac{\partial \phi_{GDL,c}}{\partial x} = \frac{\partial \phi_{e,c}}{\partial x} = \frac{\partial \phi_m}{\partial x} = 0 \tag{31}$$

2.1.4. Membrane and anode

It was assumed that there is no mass transfer of water in the membrane. Thus, the only governing equation at the membrane

is the conservation of charge:

$$\nabla^2 \phi_m = 0 \tag{32}$$

Due to significantly faster electrode kinetics and smaller mass transfer limitations compared to the cathode, the conservation equations of mass, momentum, and species are not solved at the anode. Thus also at the anode gas diffusion layer the only equation to be solved is the conservation of charge:

$$\nabla \cdot \left(-\sigma_{\mathrm{GDL},x} \frac{\partial \phi_{\mathrm{GDL,a}}}{\partial x} \vec{e}_x - \sigma_{\mathrm{GDL},y} \frac{\partial \phi_{\mathrm{GDL,a}}}{\partial y} \vec{e}_y \right) = 0 \tag{33}$$

At the anode electrode the electronic current is consumed and protonic current produced yielding:

$$\nabla \cdot (-\sigma_e \nabla \phi_{e,a}) = -j_a \tag{34}$$

$$\nabla \cdot (-\sigma_m \nabla \phi_m) = j_a \tag{35}$$

where the current production at the anode is calculated from the Tafel equation:

$$j_a = \frac{j_{0,a} z F}{RT} (\phi_{e,a} - \phi_m) \tag{36}$$

2.1.5. Membrane and anode boundary conditions

It is assumed that there is no contact resistance for protonic current at the interfaces between membrane and electrode, and thus the protonic potential is continuous over boundary XII. Boundary conditions for electronic current at the anode electrode and GDL are similar to those at the cathode. The contact resistances at the interfaces between electrode and GDL, and current collecting rib and GDL yield conditions for boundaries XIII and VIII:

$$i = -\sigma_{\mathrm{GDL},y} \frac{\partial \phi_{\mathrm{GDL,a}}}{\partial y} = -\sigma_e \frac{\partial \phi_{e,a}}{\partial y} = \frac{\phi_{\mathrm{GDL,a}} - \phi_{e,a}}{r_{\mathrm{cont,e}}} \tag{37}$$

$$i = -\sigma_{\mathrm{GDL},y} \frac{\partial \phi_{\mathrm{GDL,a}}}{\partial y} = \frac{\phi_{0,a} - \phi_{\mathrm{GDL,a}}}{r_{\mathrm{cont,gr}}} \tag{38}$$

Because the mass transfer at the anode was neglected, the interface between the GDL and gas channel (boundary IX) has only a no current condition:

$$\frac{\partial \phi_{\mathrm{GDL,a}}}{\partial y} = 0 \tag{39}$$

Finally, the symmetry boundary conditions apply again at boundaries V–VII:

$$\frac{\partial \phi_m}{\partial x} = \frac{\partial \phi_{e,a}}{\partial x} = \frac{\partial \phi_{\mathrm{GDL,a}}}{\partial x} = 0 \tag{40}$$

2.1.6. Effect of inhomogeneous compression

Due to the inhomogeneous compression of the gas diffusion layer its properties are changed. The affected GDL properties are porosity, permeability, in- and through-plane bulk conductivities, and contact resistance between gas diffusion layer and electrode interface. These changes are taken into account in the modeled cathode domain B of Fig. 1b. Cathode domain A remains unchanged compared to the base case of Fig. 1a. Because mass transfer is considered negligible at the anode, the effect of the porosity and permeability changes can be neglected there. The only differences at the anode compared to the base case are the varying bulk conductivities of GDL and contact resistance at GDL/electrode interface due to inhomogeneous compression.

The results of the measurements in the experimental part [6] imply that the gas diffusion layer is very little compressed in the middle of the channel, and that the total change from the original uncompressed volume remains small. Thus, the thickness of the gas diffusion layer in the cathode domain B is modeled with a logarithmic curve having a maximum that corresponds to 10 μm compression from the original thickness h_0. The curve was fitted so that it coincides with the constant compressed thickness h_{comp} at the point where the gas channel ends and current collecting rib begins, and equals the maximum thickness in the middle of the channel, i.e. at the right boundary III. The resulting function for gas diffusion layer thickness implemented into the model geometry coordinates is

$$h(x)\,[\mathrm{m}] = \begin{cases} h_{\mathrm{comp}}, & x \in A \\ 19.30314 \log((x - 0.0005) \times 10^6 + 1) \times 10^{-6} + h_{\mathrm{comp}}, & x \in B \end{cases} \tag{41}$$

It is assumed that the change in thickness under compression is due to change in volume of pores, not in volume of bulk material. Thus, the porosity of the GDL can be calculated from the thickness as

$$\varepsilon(x) = \varepsilon_0 \frac{h(x) - h_{\min}}{h_0 - h_{\min}} \tag{42}$$

where $h_{\min}$ equals the minimum thickness when there is only bulk material left, i.e.:

$$h_{\min} = (1 - \varepsilon_0) h_0 \tag{43}$$

A third degree polynomial fit was made with the least square sum method to the permeability data from the measurements [6], and the yielding function (fitting accuracy of $R^2 = 0.994$) for GDL is

$$k(x)\ [\mathrm{m}^2] = -1.700 \times 10^{-11} + 2.760 \times 10^{-7} h(x) - 1.484 \times 10^{-3} h(x)^2 + 2.754 h(x)^3 \tag{44}$$

The GDL in- and through-plane bulk conductivities were modeled as linear fits from the experimental data (fitting accuracies of $R^2 = 1.000$ and 0.975, respectively), and they were

$$\sigma_{\mathrm{GDL},x}(x)\,[\Omega^{-1}\,\mathrm{m}^{-1}] = 6896 - 1.159 \times 10^7 h(x) \tag{45}$$

$$\sigma_{\mathrm{GDL},y}(x)\,[\Omega^{-1}\,\mathrm{m}^{-1}] = 3285 - 8.385 \times 10^6 h(x) \tag{46}$$

An exponential fit for the experimental data ($R^2 = 0.983$) of the contact resistance between GDL and current collecting rib gave

$$r_{\mathrm{cont,gr}}(x)\,[\Omega\,\mathrm{m}^2] = 5.83 \times 10^{-10} \exp(2.06 \times 10^4 h(x)) \tag{47}$$

Because the experimental data of the contact resistance at GDL/electrode interface was unreliable, it was determined from

Table 1
Dimensions of the modeled geometries

Parameter	Symbol	Value
Channel and rib width	d	1 mm
Uncompressed GDL thickness	h_0	380 μm
Compressed GDL thickness	h_{comp}	250 μm
Electrode thickness		10 μm
Membrane thickness		25 μm

the contact resistance of GDL/rib interface. A correction factor for the Nafion content of the electrode, typically approximately 30 vol.%, was used because Nafion does not conduct electrons. Thus, the used function for contact resistance was

$$r_{\mathrm{cont,e}}(x)\,[\Omega\,\mathrm{m}^2] = \frac{1}{1-0.3} r_{\mathrm{cont,gr}}(x) = 1.429 r_{\mathrm{cont,gr}}(x) \quad (48)$$

The above-listed parameter values for domain A and for the base case were calculated from the fitted equations in order to have continuous and similar parameter values between different domains and models.

2.2. Parameters and model solving

The dimensions of the modeled geometries are given in Table 1. The constants and parameters used in the model are listed in Table 2. Standard textbook values for constants and typical values found in the PEMFC modeling articles for fuel cell parameters are used when a reference is not given.

The modeling was done using a commercial finite element method program COMSOL Multiphysics version 3.2b (formerly known as FEMLAB) with a parametric nonlinear direct (UMFPACK) solver. When solving the model, the cell voltage was used as a fixed parameter by setting the potential of anode current collector to zero and the potential of cathode current collector to cell voltage. The used mesh consisted of 24,089 elements for base case and 24,420 elements for the case where inhomogeneous compression was taken into account. The respective degrees of freedom were 36,383 and 46,443.

Table 2
Constants and parameter values

Parameter	Symbol	Value
Ambient pressure	p_0	101,325 Pa
Binary diffusion coefficient O_2,H_2O	$D^0_{O_2,H_2O}$	3.98×10^{-5} m^2 s^{-1}
Binary diffusion coefficient O_2,N_2	$D^0_{O_2,N_2}$	2.95×10^{-5} m^2 s^{-1}
Binary diffusion coefficient H_2O,N_2	$D^0_{H_2O,N_2}$	4.16×10^{-5} m^2 s^{-1}
Conductivity of electrode	σ_e	300 Ω^{-1} m^{-1} [6]
Exchange current density, cathode	$j_{0,c}$	20×10^3 A m^{-3}
Exchange current density, anode	$j_{0,a}$	1.7×10^9 A m^{-3}
Faraday constant	F	96,487 A s mol^{-1}
Gas constant	R	8.314 J mol^{-1} K^{-1}
Molar mass of oxygen	M_{O_2}	0.032 kg mol^{-1}
Molar mass of water	M_{H_2O}	0.018 kg mol^{-1}
Molar mass of nitrogen	M_{N_2}	0.028 kg mol^{-1}
Permeability of electrode	k_e	1.26×10^{-13} m^2 [10]
Porosity of uncompressed GDL	ε_0	0.84 [11]
Porosity of electrode	ε_e	0.4
Protonic conductivity	σ_m	5 Ω^{-1} m^{-1}
Reaction symmetry factor	α_r	0.5
Reversible cell potential	E_0	1.23 V
Temperature	T	323.15 K
Viscosity of air	μ	1.9×10^{-5} kg m^{-1} s^{-1}

3. Results

The polarization curves of the both simulated geometries are illustrated in Fig. 2. These were achieved by changing the cell voltage in steps of 0.1 V and calculating the average current density at each voltage over boundary X as

$$i_{\mathrm{ave}} = \frac{1}{d}\int_0^d \frac{1}{r_{\mathrm{cont,e}}}(\phi_{\mathrm{e,c}} - \phi_{\mathrm{GDL,c}})\,\mathrm{d}x \quad (49)$$

There are no significant differences between the modeled cases at practical cell voltages implying that the overall cell

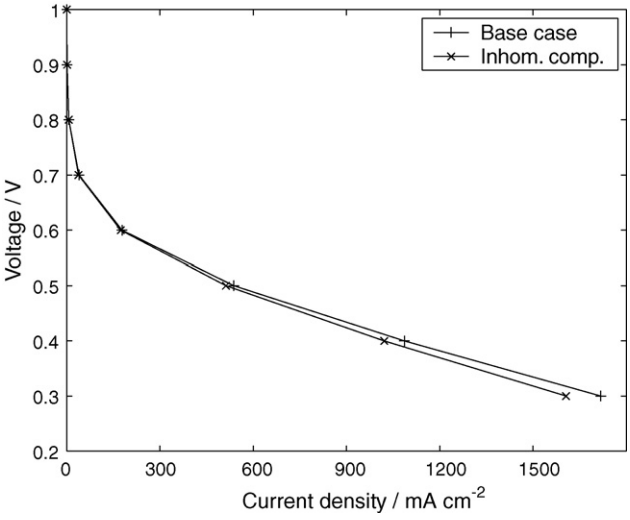

Fig. 2. Polarization curves.

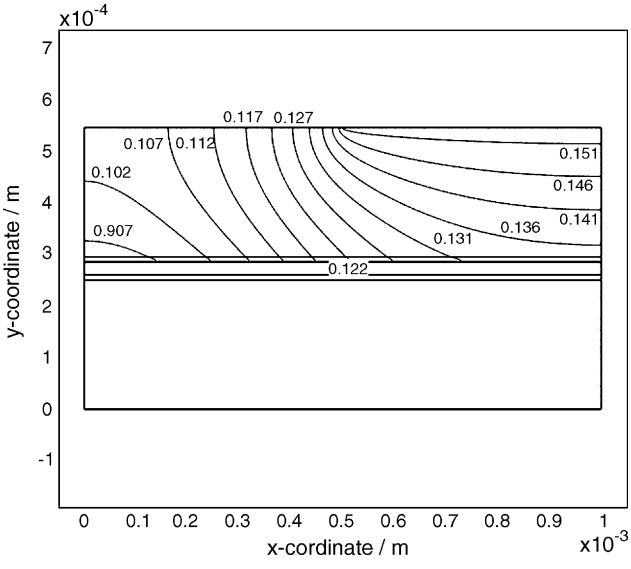

Fig. 3. Oxygen molar fraction at 0.4 V for the base case.

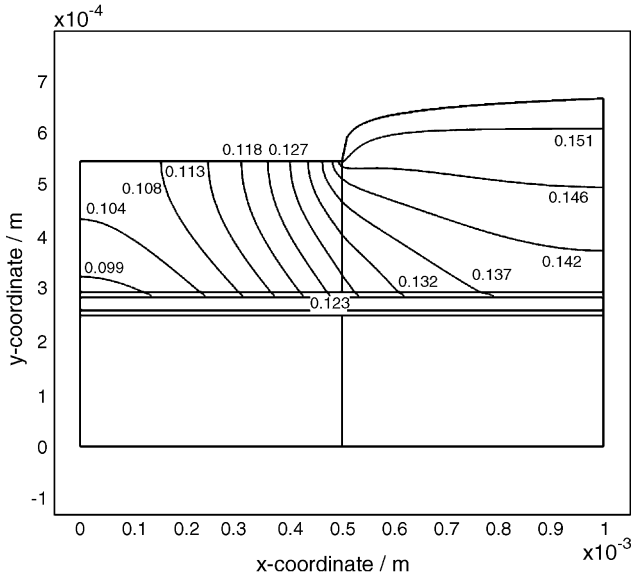

Fig. 4. Oxygen molar fraction at 0.4 V when the inhomogeneous compression is taken into account.

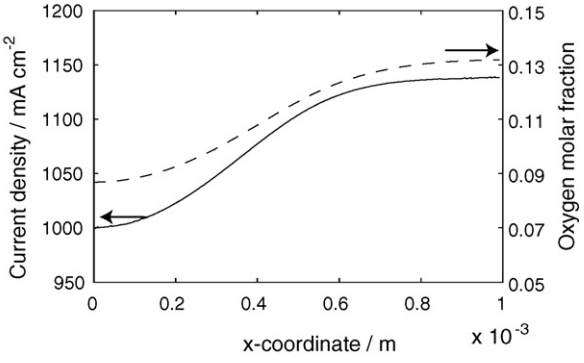

Fig. 5. Current density distribution and oxygen molar fraction at the GDL/electrode interface at 0.4 V for the base case.

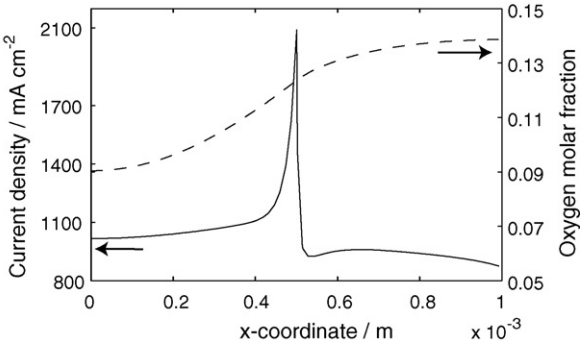

Fig. 6. Current density distribution and oxygen molar fraction at the GDL/electrode interface at 0.4 V when the inhomogeneous compression is taken into account.

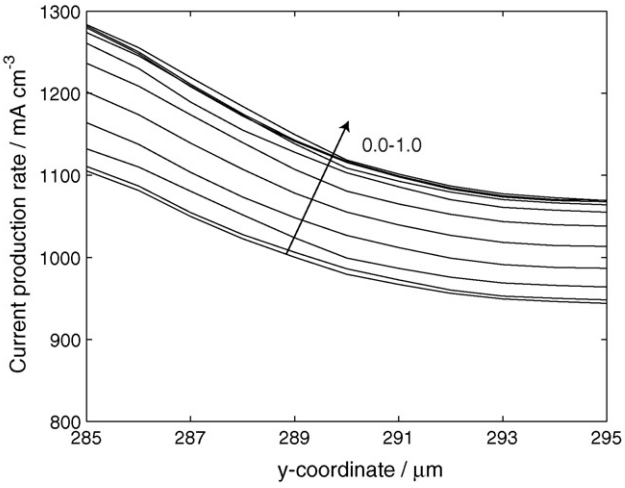

Fig. 7. Current production profiles at the electrode at 0.4 V for the base case. The profiles are current production rates in *y*-direction drawn at every 0.1 mm in *x*-direction. The arrow in the figure shows the direction of increasing *x*-axis.

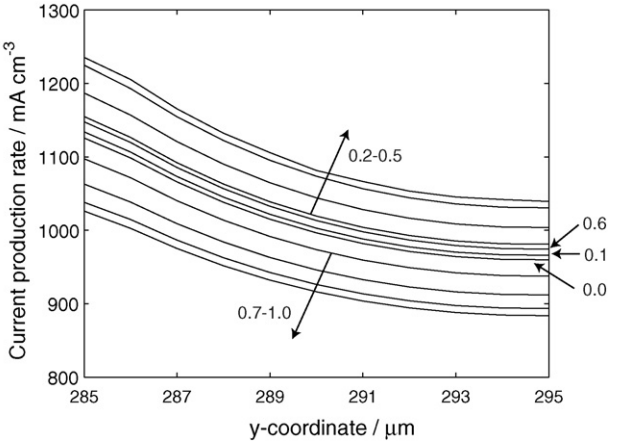

Fig. 8. Current production profiles at the electrode at 0.4 V when the inhomogeneous compression is taken into account. The profiles are current production rates in *y*-direction drawn at every 0.1 mm in *x*-direction. The arrows and labels in the figure show the direction of increasing *x*-axis and corresponding values in millimeters.

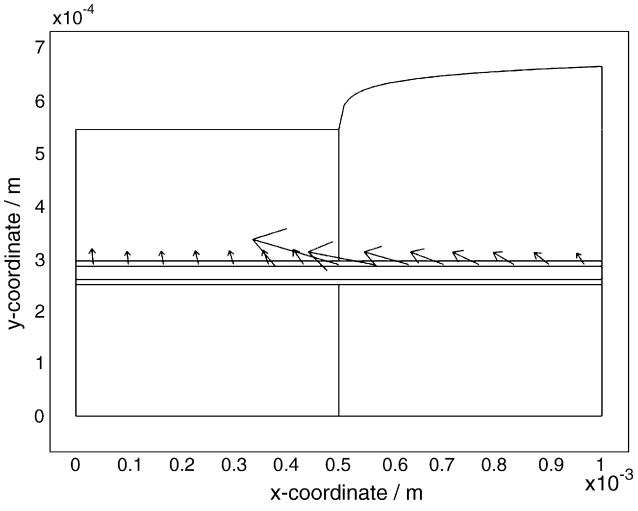

Fig. 9. Current density profile in the cathode electrode at 0.4 V when the inhomogeneous compression is taken into account.

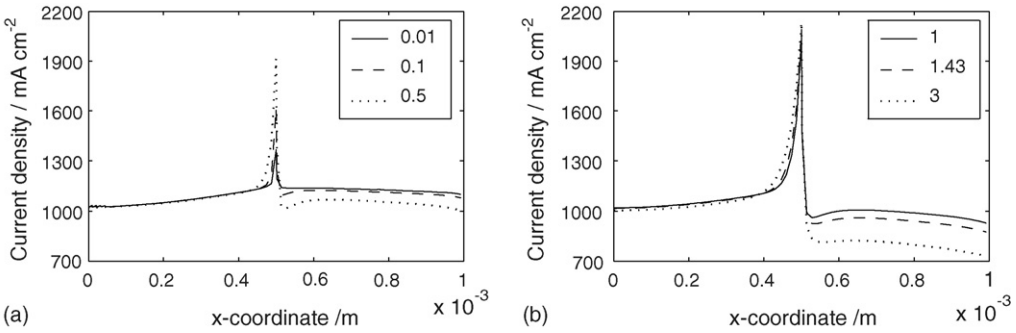

Fig. 10. Current density distributions at the GDL/electrode interface at 0.4 V with varying contact resistance values between GDL and electrode when the inhomogeneous compression is taken into account: (a) $r_{cont,e} = 0.01r_{cont,gr}$, $0.1r_{cont,gr}$, and $0.5r_{cont,gr}$; (b) $r_{cont,e} = r_{cont,gr}$, $1/(1-0.3)r_{cont,gr}$, and $3r_{cont,gr}$.

performance is not significantly affected by the inhomogeneous compression of GDL.

The differences in oxygen molar fractions between the modeled cases were also quite small. As an example, the contour plots of oxygen molar fraction at cell voltage of 0.4 V are illustrated in Figs. 3 and 4. When the inhomogeneous compression is taken into account, the equimolar lines are slightly more vertical and shifted towards the parts below the current collecting rib. For example, there is only a 5% difference in oxygen molar fraction at the GDL/electrode interface below the middle of the channel at 0.4 V. There is also no significant difference when the liquid water saturation begins (at the electrode/membrane interface below the middle of the rib) between the modeled cases, being 519 mV for the base case and 513 mV when the inhomogeneous compression is taken into account.

The small differences in mass transfer are due to relatively high open porosity and permeability of the used GDL. With another GDL material that has a microporous layer and denser structure, the differences in mass transfer are most probably more pronounced. In addition, the capillary movement of liquid water was neglected, and thus the mass transfer at low cell voltages is somewhat distorted.

Even though there were no significant differences in the overall cell performance and molar fractions between the different modeled cases, the current density distribution is significantly affected by the inhomogeneous compression. The current density profiles at GDL/electrode surface at 0.4 V are illustrated in Figs. 5 and 6. Also the oxygen molar fractions at the same interface are illustrated in the figures.

The shape of the current density distribution follows quite much the oxygen molar fraction profile in the base case, which is a very typical modeling result. When the inhomogeneous compression of GDL is taken into account, there is a significant increase in the current density below the position where the channel begins. This increase is not due to numerical inaccuracies of the solution, because the shape of the peak was unaffected by the density of the mesh.

The current production profiles, illustrated in Figs. 7 and 8, show that there are significant differences in the reaction rates between the modeled cases. The reaction rate is decreased below the channel when the inhomogeneous compression is taken into account because of higher resistive losses. However, the differences in reaction rates are quite moderate compared to current density distribution in order to explain the observed peak in Fig. 6.

The reason for the peak is illustrated in Fig. 9, where the current density profile in the cathode electrode is plotted. A significant portion of the current produced in the parts below the channel flows in-plane in the electrode and enters the GDL from the part where the contact resistance is decreased. This phenomenon obeys the second Kirschoff law: the amount of current going through a certain route is inversely proportional to the total resistance of that route. Even though the contact resistance value between GDL and electrode was estimated from the contact resistance between GDL and graphite, the effect exists even if the value was highly overestimated. This is due to the fact that when the total resistive losses under the channel are increased, a bigger portion of the produced current flows laterally in the electrode towards the smaller resistance. This phenomenon is illustrated in Fig. 10, where the current density distribution is calculated with several different contact resistance values ranging from $0.01r_{cont,gr}$ to $3r_{cont,gr}$. The current density distribution is somewhat smoothened when the contact resistance is decreased, but even at two orders of magnitude smaller value, the distribution is still highly peaked. The average current density values between different cases vary from 966 to 1113 mA cm^{-2} between the highest and lowest contact resistance values, respectively.

4. Summary and discussion

This paper focused on modeling the effects that the inhomogeneous compression of gas diffusion layer has on the performance of a PEMFC. Model took into account the multicomponent mass transfer in the cathode components and charge transfer in all of the cell components. Model was isothermal and the capillary movement of liquid water was not taken into account. The experimental parameters evaluated in Ref. [6] were used in the model, and the results were compared with a conventional model that excludes the effects of inhomogeneous compression.

There were no significant differences in the overall cell performance between the modeled cases. In addition, the mass transfer was not significantly affected by the inhomogeneous compression, which was due to the used highly porous and per-

meable GDL. This may not be the case when a denser GDL material with a microporous layer is used, because then the differences in mass transfer are pronounced. In addition, the capillary movement of liquid water was neglected and thus the mass transfer at low cell voltages was somewhat distorted.

The effect of inhomogeneous compression on the reaction rate was evident. The reaction rate was decreased under the channel because of higher total losses caused by increased bulk and contact resistances. Besides affecting the reaction rate, the effect of inhomogeneous compression on current distribution was tremendous. The current density distribution on the GDL/electrode interface was peaked at the parts below the edge of the channel. This was due to redistribution of the current profile in the electrode. A significant portion of the current flowed in in-plane direction in the electrode, and entered the GDL below the rib where there was significantly lower contact resistance. This phenomenon was investigated with several different contact resistance values between GDL and electrode, and even with very small values the current density distribution was significantly peaked.

In the model it was assumed that there is a sharp edge in the shape of the GDL at the rib/channel interface. Even though the measurement results in Ref. [6] implied that the GDB is virtually not compressed below the channel, the edge is not necessarily that sharp in reality. This is especially the case when molded composite flow-field plates with slightly rounded corners are used. However, this causes that the changes in GDL properties under the channel are not that drastic only under the rounding and thus has only a small effect on the current density distribution by slightly widening the peak to the right and rounding the tip of the peak.

The observed current density peak can have tremendous effects not only on current density distribution, but also to temperature distribution inside the cell. According to the analogy between charge and heat transfer, it can be assumed that also a significant portion of the heat produced in the electrode below the channel flows in in-plane direction. This means that there has to be a lateral temperature gradient within the electrode causing a possible hot spot below the channel. In addition, the Ohmic heating at the place where most of the current enters the GDL causes another possible hot spot below the place where the rib begins. This uneven temperature distribution can have significant effects on cell lifetime and the local cell performance. In the optimization of the PEMFC design the effect of these possible hot spots should be minimized by minimizing the parts that have low compression pressure, but in a way that efficient mass transfer is simultaneously ensured.

It was shown in this paper that the inhomogeneous compression of GDL cannot be neglected. In addition, in order to reveal the possible hot spots caused by the lateral current and heat flow in the electrode, also the electrodes have to modeled as a separate domains, i.e. modeling the electrodes as boundary conditions as sometimes is done is not a valid approach. In order to achieve reliable estimates for the temperature distribution, the energy equations have to be included in the model. Before this can be accomplished, accurate evaluation of the GDL bulk and contact heat transfer parameters as a function of thickness is required.

Acknowledgements

The financial support of the National Technology Agency of Finland (TEKES) and the Academy of Finland (project decision no. 206132) is gratefully acknowledged.

References

[1] W.-K. Lee, C.-H. Ho, J.W. Van Zee, M. Murthy, J. Power Sources 84 (1999) 45–51.
[2] J. Ge, A. Higier, H. Liu, J. Power Sources 159 (2006) 922–927.
[3] P. Zhou, C.W. Wu, G.J. Ma, J. Power Sources 129 (2006) 1115–1122.
[4] W. Sun, B.A. Peppley, K. Karan, J. Power Sources 144 (2005) 42–53.
[5] P.C. Sui, N. Djilali, J. Power Sources 161 (2006) 294–300.
[6] I. Nitta, T. Hottinen, O. Himanen, M. Mikkola, Inhomogeneous compression of PEMFC gas diffusion layer. Part I. Experimental, J. Power Sources, submitted for publication.
[7] M.J. Lampinen, Kemiallinen termodynamiikka energiatekniikassa, vol. 90, Publications of Helsinki University of Technology, Laboratory of Applied Thermodynamics, Finland, 1996 (in Finnish).
[8] R. Taylor, R. Krishna, Multicomponent Mass Transfer, John Wiley & Sons Inc., New York, 1993.
[9] J.R. Welty, C.E. Wicks, R.E. Wilson, Fundamentals of Momentum, Heat, and Mass Transfer, 3rd ed., John Wiley & Sons Inc., New York, 1984.
[10] O. Himanen, T. Hottinen, M. Mikkola, V. Saarinen, Electrochim. Acta 52 (2006) 206–214.
[11] Manufacturer's data sheet for ®Sigracet GDL 10 BA by SGL Carbon AG.